V European Conference on Computational Fluid Dynamics
ECCOMAS CFD 2010
J. C. F. Pereira and A. Sequeira (Eds)
Lisbon, Portugal,14-17 June 2010

AN IMPLICIT LOW-DIFFUSIVE HLL SCHEME FOR CAVITATING FLOW SIMULATION

M. Bilanceri*, F. Beux† and M.V. Salvetti*

*Dipartimento di Ingegneria Aerospaziale, Università di Pisa
Via G. Caruso 8, 56122 Pisa, Italy
e-mail: {m.bilanceri,mv.salvetti}@ing.unipi.it
†Alta S.p.A., Via Gherardesca, 5 - 56121 Ospedaletto, Pisa, Italy
e-mail: f.beux@alta-space.com

Key words: Cavitating barotropic flows, low-diffusive, HLL scheme, implicit time advancing, time flux linearization

Abstract. *A numerical method for generic barotropic flows is presented, together with its application to the simulation of cavitating flows. A homogeneous-flow cavitation model is indeed considered, which leads to a barotropic state equation. The continuity and momentum equations for compressible flows are discretized through a mixed finite-element/finite-volume approach, applicable to unstructured grids. P1 finite elements are used for the viscous terms, while finite volumes for the convective ones. The numerical fluxes are computed by shock-capturing schemes and ad-hoc preconditioning is used to avoid accuracy problems in the low-Mach regime. A HLL flux function for barotropic flows is proposed, in which an anti-diffusive term is introduced to counteract accuracy problems for contact discontinuities and viscous flows typical of this class of schemes, while maintaining its simplicity. Second-order accuracy in space is obtained through MUSCL reconstruction. Time advancing is carried out by an implicit linearized scheme. For this HLL-like flux function two different time linearizations are considered; in the first one the upwind part of the flux function is frozen in time, while in the second one its time variation is taken into account. The low-diffusivity characteristics of the LD-HLL scheme are first assessed for the classical case of Blasius boundary-layer. The Roe flux function is also considered for comparison. It is shown that the anti-diffusive term introduced in the HLL scheme is actually effective to obtain good accuracy (similar to the one of the Roe scheme) for viscous flows. Then, the results of the simulations of the flow around a hydrofoil mounted in a tunnel are shown, both in cavitating and non-cavitating conditions. It is shown that the more complete time linearization is a key ingredient to largely improve numerical stability and efficiency in cavitating conditions.*

1 INTRODUCTION

The prediction and characterization of cavitating flows, which occur in several engineering devices (e.g. turbomachinery, hydrofoils, marine propellers, etc), is of great importance, since cavitation has strong effects on performance and life of such devices.

From a physical view point, cavitating flows are characterized by different phenomena interacting each other, such as change of phase, complex interactions between vapor and liquid, unsteady and not well defined vapor to liquid interfaces, turbulence. All this renders the modeling of cavitating flows a very complex task. Several models exist in the literature of different levels of complexity (see [1] for a brief review). Among them are the so-called *one-fluid or equivalent-fluid* models, in which the cavitating flow is described in terms of a single fluid or mixture, whose properties are derived through suitable assumptions, and, more particularly, the *barotropic homogeneous fluid* models, in which the density and the pressure are linked each other through an equation of state, both for pure liquid and for the liquid-vapor mixture (see e.g. [2, 3, 4, 5]). The models of this kind, although they introduce rather strong simplifications and neglect a fine description of the local behavior of cavitation, are attracting because of their simplicity and because they a-priori have the capability of describing the large-scale effects of cavitation, which are dominating in many applications of interest, such as for instance in the field of rocket propulsion. In spite of the simplifying assumptions made and the apparent simplicity of such models, strong difficulties arise for numerical simulation, which are mainly due to the fact that the cavitating mixture is described as a highly compressible fluid, characterized by speed of sound values of several orders of magnitude lower that those of the pure liquid. Moreover, an abrupt transition from the wetted (incompressible) to the cavitating (highly supersonic) regimes occurs.

In this context, the present work is part of a research activity aimed at developing a numerical set-up for the simulation of flows characterized by a generic barotropic equation of state [1, 6, 7]. For the particular application to cavitating flows, a homogeneous-flow model explicitly accounting for thermal cavitation effects and for the concentration of the active cavitation nuclei in the pure liquid proposed in [3] was adopted. For cavitating flow simulation, it is clear that the numerical schemes must be designed in order to cope with nearly incompressible and highly-compressible regions coexisting in the flow. Two opposite approaches can be found in the literature: adaptation to compressible flows of methods developed for incompressible flows or adaptation to the incompressible limit, usually through ad-hoc preconditioning, of compressible flow solvers. The latter approach was used in our previous works and a preconditioned linearized implicit numerical method for the simulation of compressible barotropic flows on unstructured grids was developed, in which the spatial discretization of the convective terms is carried out through a finite-volume approach. The Roe numerical flux function [8] was adapted to barotropic flows while a Turkel-like preconditioning was considered to deal with low Mach number regime [1, 6]. Second-order spatial accuracy is obtained through the MUSCL reconstruction tech-

nique [9]. As for time advancing, a linearized implicit algorithm was defined by considering a Jacobian-free linearization of fluxes only relying on the properties of the Roe matrix [1, 6]. This linearized implicit formulation was then associated to a defect-correction technique to obtain second-order accuracy (both in time and space) at limited computational costs [7]. The set-up numerical tool was tested for different types of barotropic equations of state and flow regimes, and this validated most of the used ingredients, as, for instance, the accuracy and efficiency in the low Mach regime [1] or 2nd-order accuracy in time and space [7]. In [6], an application to the simulation of the inviscid flow in a realistic configuration of a rocket turbopump inducer in non-cavitating conditions is described. However, for cavitating flows, the stability properties of the scheme were found to deteriorate dramatically and only very small time steps are allowed. This clearly increases the computational costs and, thus, makes difficult to afford the simulation of complex cavitating flows, as occur in many aerospace and industrial applications. A rather strong reduction of the CFL number allowed by numerical stability was also recently observed in [10] for a linearized implicit time-advancing scheme, when passing from non-cavitating to cavitating conditions.

Two new ingredients are introduced and investigated herein, in order to counteract with these efficiency limitations. First, a different numerical flux function is used for the convective fluxes. The starting point is the Rusanov numerical flux function (see e.g. [11]), which is the simplest scheme of the HLL family [12]. This scheme is known to have excellent robustness properties and is attracting because of its simplicity. A preliminary study [13] was carried out in this direction showing promising results. However, the Rusanov flux as well all the HLL schemes are also known for their excessive diffusive behavior in presence of a contact discontinuity and they are, thus, not well suited for viscous flow simulations. To avoid this problem, more complex average-state approximate Riemann solvers have been introduced as, for instance, the HLLC scheme, proposed in [12], which involves two intermediate states in the approximate solution. Alternatively, an anti-diffusive term for the contact discontinuity can be directly added in the single-state HLL formulation as done in the HLLEM [14] and HLLE+ [15] schemes. In the present work, on the basis of the observation that in the 1D Riemann problem for barotropic flows density, velocity and pressure are continuous across the contact discontinuity, and thus, the presence of two different intermediate states is only due to the passive scalar (see [1, 7] for details on the Riemann problem for barotropic flow), an anti-diffusive term only acting in the passive scalar equation is introduced. This leads to a low-diffusive HLL (LD-HLL) scheme, in which the first two equations, which are related to the acoustic waves, are unchanged with respect to the original Rusanov scheme. Thus, the simple structure of the Rusanov scheme is maintained in the LD-HLL one. The second point investigated herein is the linearization in time of the numerical flux function, which is needed in order to avoid the solution of a non-linear system at each time step of the implicit algorithm. A classical linearization consists in applying a first-order Taylor expansion in time but with a complete differentiation only for the centered part of the numerical flux function while

the matrix in the upwind part is frozen at the previous time (see, e.g., [16]). Even if this choice of linearization is in general a reasonable one, the time variation of the upwind part of the flux can be large in presence of huge variations of the flow velocity or when the speed of sound has a stiff change in magnitude. The latter is a typical situation in presence of cavitation. Hence, a more complete time linearization of the LD-HLL flux is proposed herein. Thanks to the simple structure of this scheme, the time variation of the upwind terms of the flux function is analytically derived while some simplifications are made on the basis of physical considerations suitable for the cavitating case.

Finally, with respect to our previous works in which only inviscid flows were considered, the implementation of viscous effects is carried out herein through a mixed finite-volume/finite-element approach in which P1 finite elements are considered for the discretization of viscous terms.

Two test-cases are considered to investigate the effects of the previously described new numerical ingredients; the first one is aimed at investigating the effects of the anti-diffusive term introduced in the LD-HLL scheme is the classical Blasius boundary layer over a flat plate. Comparison with exact solutions and with the results given by the Roe scheme are provided. The second test-case is aimed at investigating the accuracy, robustness and efficiency properties of the Roe and the LD-HLL schemes in cavitating conditions is the flow around a NACA0015 hydrofoil mounted in a wind tunnel, for which experimental data are available [17]. For the LD-HLL scheme, the effects of the more complete time linearization are investigated. In particular, it is shown that this is a key point to largely improve the efficiency in cavitating conditions.

2 PHYSICAL MODELING

The 3D Navier-Stokes equations for a barotropic flow are considered as governing equations. By virtue of the barotropic equation of state (EOS) adopted here (see below), the energy balance is decoupled from the mass and momentum balances and therefore, it is possible to consider the following reduced set of governing equations:

$$\frac{\partial W}{\partial t} \; + \; \mathrm{div}\left(\vec{\mathcal{F}}(W) \; - \mu\vec{\mathcal{V}}(W,\nabla W)\right) = 0 \tag{1}$$

where $W = (\rho, \rho u, \rho v, \rho w)^T$, ρ being the fluid density and u, v and w the velocity components in the x, y and z directions. The vector $\vec{\mathcal{F}}(W) = (F_x, F_y, F_z)^T$ contains the classical convective flux functions for mass and momentum balances, while $\vec{\mathcal{V}}(W, \nabla W) = (V_x, V_y, V_z)^T$ are the corresponding viscous fluxes and μ is the fluid viscosity.

The 1D inviscid case is used as a first step for the definition of the different numerical approaches, which are then extended and implemented in the 3D viscous case. Thus, the following 1D flow system is also considered:

$$\frac{\partial W}{\partial t} \; + \; \frac{\partial F(W)}{\partial x} = 0 \tag{2}$$

where $W = (\rho, \rho u, \rho\xi)^T$ and $F(W) = (\rho u, \rho u^2 + p, \rho u\xi)^T$ in which p is the pressure and ξ denotes a passive scalar.

For the development of the numerical methods a generic barotropic equation of state, i.e. $p = p(\rho)$, is considered. The derivative $dp/d\rho$ is assumed to be strictly positive (a classical thermodynamic stability requirement for common fluids) and can be regarded as the square of the fluid sound speed $a(\rho)$.

For cavitating flow simulations, a weakly-compressible liquid at constant temperature T_L is considered as working fluid. The liquid density ρ is allowed to locally fall below the saturation limit $\rho_{Lsat} = \rho_{Lsat}(T_L)$ thus originating cavitation phenomena. A regime-dependent (wetted/cavitating) constitutive relation is therefore adopted.

As for the wetted regime ($\rho \geq \rho_{Lsat}$), the chosen model is of the form:

$$p \;=\; p_{sat} \;+\; \frac{1}{\beta_{sL}} \;\ln\left(\frac{\rho}{\rho_{Lsat}}\right) \tag{3}$$

$p_{sat} = p_{sat}(T_L)$ and $\beta_{sL} = \beta_{sL}(T_L)$ being the saturation pressure and the liquid isentropic compressibility, respectively.

Concerning the cavitating regime ($\rho < \rho_{Lsat}$), a homogeneous-flow model explicitly accounting for thermal cavitation effects and for the concentration of the active cavitation nuclei in the pure liquid has been adopted [3]:

$$\frac{p}{\rho}\frac{d\rho}{dp} = (1-\alpha)\left[(1-\varepsilon_L)\frac{p}{\rho_{Lsat}a_{Lsat}^2} + \varepsilon_L g^\star\left(\frac{p_c}{p}\right)^\eta\right] + \frac{\alpha}{\gamma_v} \tag{4}$$

where $g^\star$, η, γ_V and p_c are constant parameters depending on the substance considered, a_{Lsat} is the liquid sound speed at saturation, and α is the void fraction defined as:

$$\alpha = \frac{\rho_{Lsat} - \rho}{\rho_{Lsat} - \rho_v} \simeq 1 - \frac{\rho}{\rho_{Lsat}} \tag{5}$$

ρ_v being the vapor density. Finally, $\varepsilon_L = \varepsilon_L(\zeta, \alpha)$ is the fraction of the liquid in thermal equilibrium with the vapor. Its expression depends on ζ a free model parameter accounting for thermal cavitation effects and, possibly, for the concentration of the active cavitation nuclei, see [3] for more details. Moreover, the fluid molecular viscosity is also expressed as a function of the void fraction with $\mu = \alpha\mu_v + (1-\alpha)\mu_L$ in which μ_v and μ_L are the molecular viscosity of the vapor and of the liquid respectively.

Note that despite the model simplifications leading to a unified barotropic EOS, the transition between wetted and cavitating regimes is extremely abrupt. Indeed, the sound speed falls from values of order 10^3 m/s in the pure liquid down to values of order 10^{-1} m/s or 1 m/s in the mixture [3, 6, 1]. The corresponding Mach number variation makes this state equation very stiff from a numerical viewpoint.

3 NUMERICAL DISCRETIZATION

The spatial discretization of the governing equations is based on a mixed finite-element/ finite-volume formulation on unstructured tetrahedral grids. Finite volumes are used for the convective fluxes, while the viscous terms are discretized through P1 finite elements. Time advancing is carried out through an implicit linearized algorithm. For sake of simplicity the main numerical ingredients are presented in details in the 1D inviscid case, the generalization to 3D viscous flow equations is then briefly discussed.

3.1 Spatial discretization: first-order schemes

The finite-volume spatial discretization of systems of hyperbolic equations as (2) leads to the following semi-discrete problem:

$$\delta x_i \frac{\mathrm{d}W_i}{\mathrm{d}t} + \Phi_{i(i+1)} - \Phi_{(i-1)i} = 0 \tag{6}$$

where δx_i is the width of the finite-volume cell i and Φ_{ij} is a numerical flux function between the i^{th} cell and the j^{th} one.

3.1.1 Approximate Riemann solvers for barotropic flows

The numerical flux functions considered herein are constructed through an approximation of the Riemann problem, by considering a linearized problem (Roe scheme) or an average-state approximation (HLL schemes). The solution for the Riemann problem with a generic convex barotropic equation of state has been described in [1] and it is composed by three waves: the intermediate one is always a contact discontinuity, the others can be shock or rarefaction waves. This simple three-waves configuration is obtained in particular for the barotropic EOS described in Sec. 2, i.e. Eqs. (3) and (4).

The Roe scheme One of the most popular choices of numerical flux function is obtained by considering the linearized approximate Riemann solver proposed by Roe [8]. In this case, Φ_{ij} can be expressed as follows:

$$\Phi_{i,j} = \frac{F(W_i) + F(W_j)}{2} - \frac{1}{2}|\tilde{J}(W_i, W_j)|(W_j - W_i) \tag{7}$$

in which the so-called Roe matrix $\tilde{J}$ is a diagonalizable matrix satisfying suitable specific properties (see [8]). For the case of a generic barotropic state equation and the 1D hyperbolic system (2), the Roe matrix has been derived in [1, 7]. The eigenvalues of this matrix are found to be $\tilde{\lambda}_1 = \tilde{u}_{ij} + \tilde{a}_{ij}$, $\tilde{\lambda}_2 = \tilde{u}_{ij} - \tilde{a}_{ij}$ and $\tilde{\lambda}_3 = \tilde{u}_{ij}$ where $\tilde{u}_{ij}$ corresponds to the well-known "Roe average" for the states W_i and W_j of u whereas $\tilde{a}_{ij}$, which can be considered as a Roe average for the sound speed, is defined as $\tilde{a}_{ij} = (p(\rho_j) - p(\rho_i))^{\frac{1}{2}}(\rho_j - \rho_i)^{-\frac{1}{2}}$ for $\rho_j \neq \rho_i$.

A simple HLL scheme The HLL schemes [18], which assume one intermediate wave state between two acoustic waves in the approximate Riemann problem, are widely used due to their simplicity, reliability and robustness. The choice of s_L and s_R, the acoustic wave speed estimates, fully determines each particular scheme. The Rusanov scheme furnishes the simplest choice by considering $s_L = -s_R$, and thus, can be expressed as:

$$\Phi_{i,j} = \frac{F(W_i) + F(W_j)}{2} - \frac{\lambda_{ij}}{2}(W_j - W_i) \tag{8}$$

where $\lambda_{ij} = s_R$ is an upper bound for the fastest wave speed. A classical choice for λ_{ij} is the largest absolute value of the Roe matrix eigenvalues.

The HLL schemes are trivially generalizable to the case of barotropic EOS. Indeed, both the acoustic wave speeds of the exact Riemann problem and the corresponding Roe matrix eigenvalues are formally identical in the barotropic and non-barotropic cases even if the definition of the sound speed is different. Thus, a Rusanov scheme for barotropic EOS is proposed, here, considering the numerical flux function (8) associated with the approximate wave speed $\lambda_{ij} = \max_p(|\tilde{\lambda}_p|) = |\tilde{u}_{ij}| + \tilde{a}_{ij}$.

A modified HLL scheme with an anti-diffusive term The HLL schemes are known for their excessive diffusive behavior in presence of a contact discontinuity. To avoid this problem, an anti-diffusive term for the contact discontinuity can be added as done with the HLLEM scheme [14] or with successive improved schemes (e.g. the HLLE+ one [15]). In this context, the following unified expression of the flux function can be used to represent HLL (taking $\bar{\delta} = 0$), HLLEM, HLLE+ as well as Roe fluxes:

$$\Phi(W_l, W_r) = \frac{b^+ F(W_l) - b^- F(W_r)}{b^+ - b^-} + \frac{b^+ b^-}{b^+ - b^-}\left((W_r - W_l) - \sum_{p \in S_{cd}} \bar{\delta}\alpha_p r_p\right) \tag{9}$$

in which b^+, b^- and $\bar{\delta}$ are parameters depending on the states W_l and W_r, while r_p are the right eigenvectors of the Jacobian matrix of the flux function F evaluated at a particular intermediate state and α_p the components of $W_r - W_l$ in the right-eigenvector basis. S_{cd} is the set of indexes for which r_p is associated with the eigenvalue u of the flux Jacobian matrix, i.e. related to the contact discontinuity. Thus, the last term in the right hand side of (9) represents an anti-diffusive term for the contact discontinuity. However, for the classical case of an ideal-gas EOS, any modification of this term acts on the whole system of equations, and consequently, the choice of an adequate parameter $\bar{\delta}$ is rather critical (see [15]). The situation is different for the barotropic case since density, velocity and pressure are continuous across the contact discontinuity, and thus, the presence of two different intermediate states is only due to the passive scalar (see [1, 7]). Moreover, only one eigenvalue is associated with the contact discontinuity while the corresponding eigenvector r_3 can be always chosen to be $(0\ 0\ 1)^T$ whatever is the particular intermediate state. Consequently, the anti-diffusive term in (9) affects only the third equation of the

system. Due to this decoupling from mass and momentum equations, there are less restrictions on the choice of $\bar{\delta}$ in the barotropic case. Clearly, it should correspond to an anti-diffusive term in order to avoid the smearing of the contact discontinuity of the HLL scheme, and on the other hand, the estimate of the wave speeds should remain as close as possible to the real ones. The simplicity of the scheme is privileged here for the choice of the modified term in view of its incorporation in the complete formulation including preconditioning for low Mach number and linearized implicit approach (see sections 3.2 and 3.3). Consequently, starting from the simplest HLL scheme, i.e. the Rusanov one, the following scheme, called in the following LD-HLL (Low-Diffusive HLL), is proposed:

$$\Phi_{i,j} = \frac{F(W_i) + F(W_j)}{2} - \frac{1}{2} \begin{pmatrix} \lambda_{ij} & 0 & 0 \\ 0 & \lambda_{ij} & 0 \\ 0 & 0 & |\tilde{u}_{ij}| \end{pmatrix} (W_j - W_i) \tag{10}$$

With respect to the original Rusanov scheme, the first two equations, which are related to the acoustic waves, are unchanged, while for the third equation, i.e. the one directly related to the contact discontinuity, the diffusive part of the scheme has been reduced. Furthermore, this scheme can also be expressed in terms of the unified Godunov-type formulation (9) by considering the following parameters:

$$b^- = -\lambda_{ij},\, b^+ = \lambda_{ij} \quad \text{and} \quad \bar{\delta} = \frac{\tilde{a}_{ij}}{\tilde{a}_{ij} + |\tilde{u}_{ij}|} \left(1 + \frac{\tilde{\xi}_{ij}(\rho_j - \rho_i)}{\tilde{\rho}_{ij}(\xi_j - \xi_i)} \right) \tag{11}$$

in which we have chosen to express $W_j - W_i$ in the basis of the Roe matrix eigenvectors.

Note that the Rusanov, Roe and LD-HLL schemes are Q-schemes, i.e. the numerical flux function can be expressed as:

$$\Phi_{ij} = \frac{F(W_i) + F(W_j)}{2} - \frac{1}{2} Q_{ij} \, (W_j - W_i) \tag{12}$$

The various schemes differ for the definition of the matrix Q_{ij} which can be directly obtained from eqs. (7), (8) and (10) respectively.

3.2 Preconditioning for low Mach number flows

For the cavitating flow problem, a large part of the flow is characterized by very low Mach numbers since we have to deal with a weakly-compressible liquid. Compressible solvers encounter accuracy problems when dealing with nearly-incompressible flows [19]. In order to counteract this difficulty, some preconditioning must be applied.

A Turkel-like preconditioning has been proposed in [1, 6] for the Roe flux function associated with a barotropic EOS using a similar formulation as proposed in [19] for a perfect-gas state equation. This preconditioning is acting only on the upwind part of the numerical flux function; more precisely, $Q_{ij} = |\tilde{J}(W_i, W_j)|$ is replaced by:

$$Q_{ij} = P_{ij}^{-1} |P_{ij} \tilde{J}(W_i, W_j)| \quad \text{with} \quad P_{ij} = \left. \frac{\partial W_p}{\partial W} \right|_{ij} \Lambda_p \left. \frac{\partial W}{\partial W_p} \right|_{ij}$$

where W_p is the vector of the primitive variables and $\Lambda_p = diag(\beta^2, 1, 1)$, the parameter β being proportional to a reference Mach number. It has been shown that the preconditioned formulation with this choice of P_{ij} does not present accuracy problems for low Mach number flows, this both from a theoretical and a numerical point of view [1, 6].

By carrying out an asymptotic analysis it has been found that the Rusanov scheme also encounters accuracy problems in the low Mach number limit [13]. However, the correct asymptotic behavior of the analytical solution can be recovered acting directly on the acoustic diagonal terms of the matrix Q_{ij}. More precisely, it is possible to consider the following "preconditioned" matrix:

$$Q_{ij} = \lambda_{ij} \begin{pmatrix} \theta^{-1} & 0 & 0 \\ 0 & \theta & 0 \\ 0 & 0 & 1 \end{pmatrix} \quad \text{with} \quad \theta = \begin{cases} 10^{-6} & \text{if } M \leq 10^{-6} \\ \\ \min(M, 1) & \text{otherwise} \end{cases} \tag{13}$$

in which M represents a local Mach number expressed with respect to the Roe average values, i.e. $M = |\tilde{u}|/\tilde{a}$. With this simple preconditioning procedure, the correct asymptotic behavior of the analytical solution is recovered (for details see [13]).
Note that since the preconditioning affects only the mass and momentum balances and not the passive scalar field, the analysis in [13] is also valid for the LD-HLL scheme (10) and thus, the "preconditioned matrix" for this scheme is:

$$Q_{ij} = \begin{pmatrix} \lambda_{ij}\theta^{-1} & 0 & 0 \\ 0 & \lambda_{ij}\theta & 0 \\ 0 & 0 & |\tilde{u}_{ij}| \end{pmatrix} \tag{14}$$

3.3 Linearized implicit time advancing

Let us consider an implicit backward Euler method applied to the semi-discrete problem (6):

$$\frac{\delta x_i}{\Delta t} \Delta^n W_i + \Delta^n \Phi_{i,i+1} - \Delta^n \Phi_{i-1,i} = -\left(\Phi^n_{i,i+1} - \Phi^n_{i-1,i}\right) \tag{15}$$

where $\Delta^n(\cdot) = (\cdot)^{n+1} - (\cdot)^n$. To avoid the solution of a non-linear system at each time step, a linearization of $\Delta^n \Phi_{ij}$ is usually adopted. A way to obtain such a linearization is to find two matrices D_1 and D_2 such that

$$\Delta^n \Phi_{ij} \simeq D_1(W^n_i, W^n_j)\, \Delta^n W_i + D_2(W^n_i, W^n_j)\, \Delta^n W_j \tag{16}$$

In this case (15) reduces to a block tridiagonal linear system.

A Jacobian-free linearization for the Roe scheme was previously derived in [1, 6, 7], which only exploits the algebraic properties of the Roe matrix and, therefore, does not depend on the specific equation of state. This approach is characterized by:

$$\begin{cases} D_1(W^n_i, W^n_j) = \tilde{J}^+(W^n_i, W^n_j) \\ \\ D_2(W^n_i, W^n_j) = \tilde{J}^-(W^n_i, W^n_j) \end{cases} \quad \text{with} \quad \tilde{J}^{\pm} = \frac{1}{2}\left(\tilde{J} \pm |\tilde{J}|\right) \tag{17}$$

However, due to its particular construction, this approach can be used only for the Roe scheme.

Alternatively, a classical linearization of type (16) consists in applying a first-order Taylor expansion in time but with a complete differentiation only for the centered part of the numerical flux function while the matrix Q_{ij} in the upwind part is frozen at time t^n (see, e.g., [16]). This results in the following approximation:

$$\Delta^n \Phi_{ij} \simeq \frac{1}{2}\left(A(W_i^n)\Delta^n W_i + A(W_j^n)\Delta^n W_j\right) - \frac{1}{2} Q_{ij}^n \left(\Delta^n W_j - \Delta^n W_i\right) \tag{18}$$

in which A is the Jacobian matrix of F. Note that this approach can be used for any upwind scheme of type (12), independently of the differentiability or of the complexity in the differentiation of Q_{ij}. Let us reinterpret this linearization by rewriting the time variation of the upwind term of Φ_{ij} as follows:

$$\Delta^n \Phi_{ij,u} = -\frac{Q_{ij}^n}{2}(\Delta^n W_j - \Delta^n W_i) - \frac{\Delta^n Q_{ij}}{2}(W_j^{n+1} - W_i^{n+1}) \tag{19}$$

The previous linearization is obtained just by neglecting the last term in the upwind part of Φ_{ij}, i.e. the second term in the right hand side of (19). It is worth noting that this term, denoted herein $\Gamma_{ij}^{n,n+1}$, can be neglected as long as that the solution is regular enough to satisfy:

$$W_j^{n+1} - W_i^{n+1} \propto O(\Delta x) \quad \text{and} \quad \Delta^n Q_{ij} \propto O(\Delta t) \tag{20}$$

Even if the assumption (20) is in general a reasonable one, there are situations of practical interest in which it is not satisfied. Indeed, if a discontinuity is present the magnitude of the term $W_j^{n+1} - W_i^{n+1}$ can be large independently of the size of Δx. Moreover, the term $\Delta^n Q_{ij}$ can also be large. This can happen, in particular, in presence of huge variations of the flow velocity or when the speed of sound has a stiff change in magnitude. The latter is a typical situation in presence of cavitation. Thus, a more complete linearization is proposed here by taking into account, at least in an approximate way, the term $\Gamma_{ij}^{n,n+1}$. This linearization can be applied for any Q-scheme as defined by (12) where Q_{ij} is a diagonal matrix such that any of its diagonal coefficient can be written as a composite function of two variables, $\bar{a}$ and $\bar{u}$, as follows:

$$q_k = q_k\left(\bar{u}\left(W_i(t), W_j(t)\right), \bar{a}\left(W_i(t), W_j(t)\right)\right) \tag{21}$$

Here, Q_{ij} could be the one of the original Rusanov scheme or alternatively the LD-HLL one, but it can also include the case with preconditioning, i.e. Q_{ij} given by (13) or (14).

Then, through differentiation of (21), by neglecting terms of higher order and after some mathematical developments (see [13]), the following approximation of the previously neglected term is obtained:

$$\Gamma_{ij}^{n,n+1} \simeq \frac{1}{2} K_{ij} \Delta^n W_i - \frac{1}{2} K_{ji} \Delta^n W_j \tag{22}$$

in which the generic element of K_{ij} is defined by the following expression:

$$\left(K_{ij}\right)_{km} = \left(\frac{\partial q_k}{\partial \bar{u}}\frac{\partial \bar{u}}{\partial W_{i,m}} + \frac{\partial q_k}{\partial \bar{a}}\frac{\partial \bar{a}}{\partial W_{i,m}}\right)\left(W^n_{j,k} - W^n_{i,k}\right) \tag{23}$$

where $W_{i,m}$ denotes the m-th element of the vector W_i. Finally, considering $\Gamma^{n,n+1}_{ij}$ from (22)-(23) in the evaluation of the upwind part of the numerical flux time variation, i.e. in (19), the following more complete approximation is obtained instead of (18):

$$\Delta^n\Phi_{ij} \simeq \frac{1}{2}\left(A(W^n_i) + Q^n_{ij} - K_{ij}\right)\Delta^n W_i + \frac{1}{2}\left(A(W^n_j) - Q^n_{ij} + K_{ji}\right)\Delta^n W_j \tag{24}$$

Note that some simplifications for the computation of the elements of matrix K_{ij} have been done through physical considerations related to the particular kind of applications of interest in this study. Then, the remaining terms are numerically computed through centered finite differences. We refer to [13] for more details.

3.4 Second-order formulation

A space and time second-order accurate approach is obtained considering a classical MUSCL reconstruction for space (see [9]) and a second-order backward differentiation formula for time advancing. Then, the following implicit formulation is considered instead of (15):

$$\delta x_i \frac{3W^{n+1}_i - 4W^n_i + W^{n-1}_i}{2\Delta t} + \Delta^n\Phi_{i+\frac{1}{2}} - \Delta^n\Phi_{i-\frac{1}{2}} = -\left(\Phi^n_{i+\frac{1}{2}} - \Phi^n_{i-\frac{1}{2}}\right) \tag{25}$$

where $\Phi_{i\pm\frac{1}{2}} = \Phi(W^-_{i\pm\frac{1}{2}}, W^+_{i\pm\frac{1}{2}})$ are the second-order accurate numerical fluxes computed by using extrapolated variable values at the cell interface. Similarly to the 1st-order case, a linearization of $\Delta^n\Phi_{i\pm\frac{1}{2}}$ must be carried out in order to avoid the solution of a non linear system at each time step. However, the linearization for the second-order accurate fluxes and the solution of the resulting linear system implies significant computational costs and memory requirements. Thus, a defect-correction technique (see e.g. [20]) is used here, which consists in iteratively solving simpler problems obtained by considering the same linearization as used for the 1st-order scheme (for more details see [7]).

3.5 Extension to 3D

In 3D, starting from an unstructured tetrahedral grid, a dual finite-volume tessellation is obtained by the rule of medians: a cell C_i is built around each vertex i, and boundaries between cells are made of triangular interface facets. Each of these facets has a mid-edge, a face centroid, and a tetrahedron centroid as vertexes.

The semi-discrete balance applied to cell C_i reads (not accounting for boundary contributions):

$$\frac{dW_i}{dt} + \frac{1}{V_i}\sum_{j\in\mathcal{K}(i)}\Phi_{ij} + \sum_{\mathcal{T}\in S_i} V(\mathcal{T})(\mu\vec{\mathcal{V}})|_{\mathcal{T}}\cdot\nabla\psi_i|_{\mathcal{T}} = 0 \tag{26}$$

where W_i is the semi-discrete unknown associated with C_i, V_i is the cell volume, $\mathcal{K}(i)$ represents the set of nodes joined to i through an edge and Φ_{ij} denotes the numerical flux crossing the boundary ∂C_{ij} shared by C_i and C_j (positive towards C_j). Once defined $\vec{\nu}_{ij}$ as the integral over ∂C_{ij} of the outer unit normal to the cell boundary, it is possible to approximate Φ_{ij} by exploiting a 1D flux function between W_i and W_j, along the direction $\vec{\nu}_{ij}$ and the extension of the schemes previously presented is straightforward. More details on the 3D formulation can be found in [6] for the formulation based on the Roe scheme. As for the viscous terms, $\mathcal{T}$ denotes the tetrahedron, S_i is the set of tetrahedrons containing the node i, $(\mu\vec{\mathcal{V}})|_{\mathcal{T}}$ is the P1 finite-element approximation of the viscous fluxes over the tetrahedron $\mathcal{T}$ and $\nabla\psi_i|_{\mathcal{T}}$ the gradient of ψ_i over the tetrahedron $\mathcal{T}$, ψ_i being the P1 basis function associated to node i.

4 NUMERICAL APPLICATIONS

4.1 Blasius boundary layer

As previously mentioned, it is well-known that due to their excessive diffusivity in presence of contact discontinuities, the HLL schemes, as the standard Rusanov one, are not well-suited for viscous flow simulation. The Blasius boundary layer can thus be considered an appropriate test to validate the effectiveness of the anti-diffusive term introduced in the LD-HLL scheme. We consider hence the laminar viscous flow along a flat plate at zero angle of attack; water at $T = 293.16K$ is used as a working fluid. The considered free-stream conditions are the following: $\rho_\infty = 998Kg/m^3$, $p_\infty = 10^5Pa$, $u_\infty = 0.01m/s$. Note that the freestream Mach number is approximately 10^{-5} and thus compressibility effects are negligible and comparison with the Blasius solution for incompressible flows can be made. The Reynolds number, based on the freestream velocity and the flat plate length, is about 10000 ($\mu = 0.001Kg/(ms)$). We remark that in this test-case no cavitation phenomena occur in the flow. A square computational domain is considered with $-1 \leq x \leq 1$ and $0 \leq y \leq 2$ where x is the streamwise direction and y the direction normal to the flat plate. The flat plate is located at $0 \leq x \leq 1$ and $y = 0$. Characteristic based boundary conditions [1] are used at the inflow ($x = -1$) and at the outflow ($x = 1$). Symmetry is imposed for $y = 0$ and $-1 < x < 0$ while no-slip conditions are considered at the flat-plate. Finally, free-slip conditions are used at $y = 2$. The independence of the results to the normal width of the domain has been checked.

The computational grids are generated as follows. Firstly, the square $0 \leq x \leq 1$ and $0 \leq y \leq 1$ is considered. The edge along the x direction is divided in a given number of segments, N_x, with length Δx varying in geometric progression with the smallest element (Δx_{min}) at the leading edge. Analogously the edge along the y direction is divided in N_y segments, with length Δy varying in geometric progression with the smallest element (Δy_{min}) at the wall. A structured quadrilateral grid is then generated and is reflected along the axis $x = 0$. For $y > 1$ the value of Δy is constant equal to the maximum value over the the square $0 \leq x \leq 1$ and $0 \leq y \leq 1$. Finally, each element of this grid is divided

in 5 tetrahedrons by an English-flag type procedure. By using the previously described procedure, two grids whose main parameters are given in Tab. 1 were obtained.

Grid	N_x	q_x	Δx_{min}	Δx_{max}	N_y	q_y	Δy_{min}	Δy_{max}
Grid1	25	1.21	1.8×10^{-3}	0.18	25	1.44	4.8×10^{-5}	0.33
Grid2	50	1.1	8.6×10^{-4}	0.1	50	1.2	2.19×10^{-5}	0.16

Table 1: Grids used for the flat plate simulations. N_x is the number of divisions of $0 \leq x \leq 1$, q_x is the ratio of the geometrical progression used for setting the length of the elements in the x direction, Δx_{min} and Δx_{max} are the minimum and maximum length of the elements in the x direction. N_y, q_y, Δy_{min}, Δy_{max} are the corresponding quantities in the y direction.

The results of the simulations with three different numerical schemes (Roe, Rusanov and LD-HLL) on grids Grid1 and Grid2 are compared and validated against the Blasius solution. Figs. 1a and 1b show the comparison of the velocity profile at section $x/c = 0.6$ while Figs. 1c and 1d show the comparison of the wall shear stress along the flat plate. Note that the velocity profile has been plotted only at one section ($x/c = 0.6$), but the same behavior is observed for any section over the plate, this in terms of grid refinement as well as for the comparison between the different numerical schemes. While the results obtained with the standard Rusanov scheme lack in accuracy even with the more refined grid and confirm its over-diffusive character, the LD-HLL scheme gives very similar results to the Roe one and in good agreement with the Blasius solution. The small discrepancies with respect to the Blasius solution tend to vanish with grid refinement for the LD-HLL and Roe approaches.

This test-case thus confirms that the anti-diffusive term introduced in the LD-HLL scheme actually counteracts the accuracy problems encountered by the standard Rusanov scheme in viscous flow simulations.

4.2 Flow around a NACA0015 hydrofoil

Test-case	U_∞ (m/s)	p_∞ (Pa)	T (K)	M_∞	$\sigma_\infty = \frac{p_\infty - p_{sat}}{1/2\rho U_\infty^2}$
TC1	3.115	59050	298.15	2.2×10^{-3}	11.71
TC2	3.46	12000	298.15	2.4×10^{-3}	1.49
TC3	3.46	11400	298.15	2.4×10^{-3}	1.38

Table 2: Inlet conditions for the flow around a NACA0015 hydrofoil.

The liquid flow over a NACA0015 hydrofoil in cavitating and non-cavitating conditions is considered. The hydrofoil of chord length c equal to 115 mm is mounted in a water tunnel at 4° incidence angle and spans the entire width of the rectangular test chamber section. The test section, which is obtained by cutting the chamber along its symmetry plane has a width of $1.28c$. This configuration has been considered in an experimental

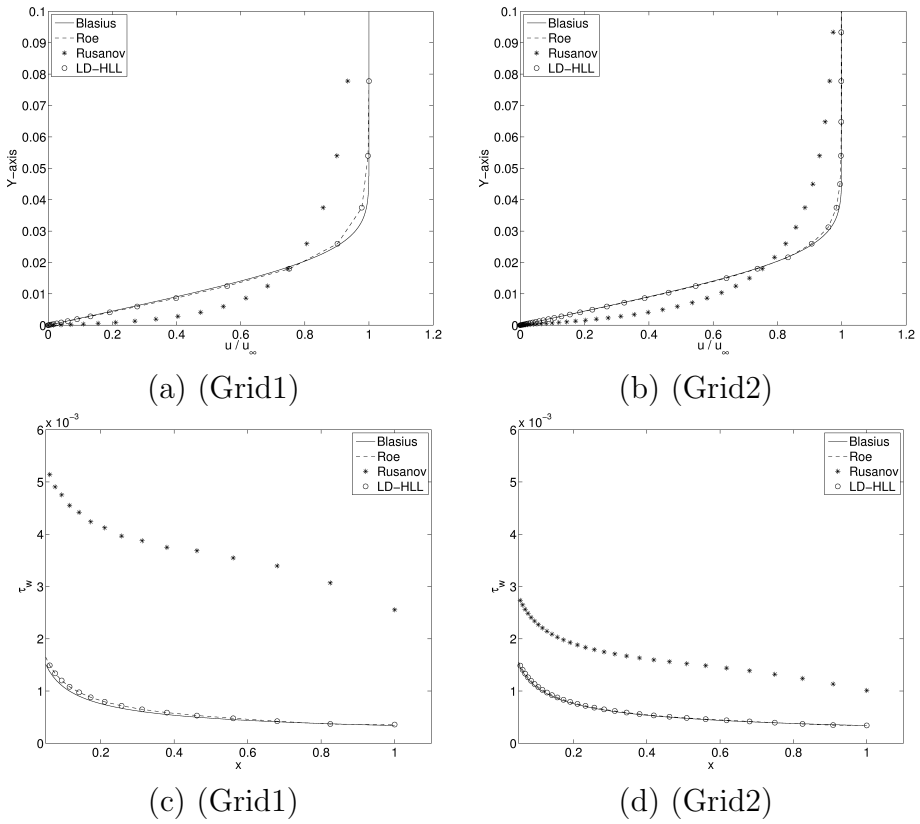

(a) (Grid1) (b) (Grid2)

(c) (Grid1) (d) (Grid2)

Figure 1: Velocity profiles at $x/c = 0.6$ (frames a and b) and wall shear stress (frames c and d) over the flat plate obtained on different grids.

study in [17] for which the pressure coefficient distribution on the symmetry plane of the hydrofoil is available. Three different sets of inlet conditions are considered as summarized in Tab. 2; the first conditions (TC1) correspond to a non-cavitating case while the second and the third ones (TC2 and TC3) generate a cavitating flow. The inlet conditions TC1 and TC2 correspond to those of the reference experiments. The equations of state (3)-(4) for cavitating flows are used by taking T_L equal the temperature T given by Tab. 2 and $\zeta = 0.01$. The dimensions of the computational domain in the lateral direction are the same of the experimental test section, while in the streamwise direction the inlet is at a distance of $3c$ from the leading edge and the outflow at a distance of $4c$ from the trailing edge. Finally, in the spanwise direction the domain thickness is $0.1c$, i.e. only a slice of the actual chamber width is considered. In [21] it was shown that this has not significant effects on the numerical pressure distribution over the hydrofoil, except for slight differences near the trailing edge. Characteristic based boundary conditions [1] are used at the inflow and outflow, while free slip is imposed at the remaining boundaries. Three different unstructured grids are considered, the first one GR1, made of 115728 nodes, is used for the non-cavitating test TC1, the second (GR2) and third (GR3) grids

are used for the cavitating cases and have 263832 and 502234 nodes respectively.

4.2.1 Results of the non-cavitating simulations

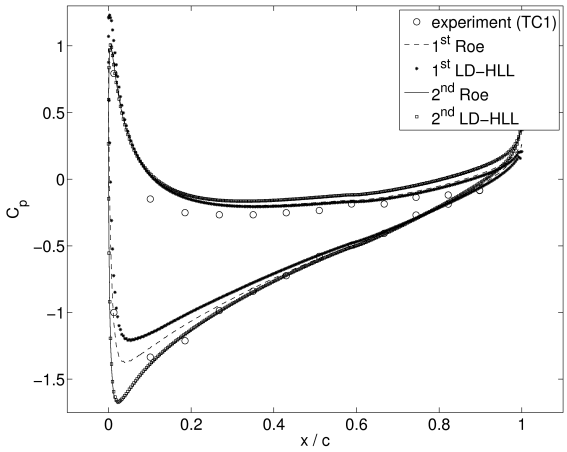

Figure 2: C_p distribution over the hydrofoil for the TC1 test-case (non-cavitating flow).

For all the considered schemes large CFL values can be used for non-cavitating flows; here, a CFL value of 200 has been chosen for the different simulations. Since this already led to very reduced computational times on the considered grid GR1, a systematic analysis of the actual stability limit has not been carried out for these simulations.

The pressure coefficient distributions obtained on the hydrofoil in the simulations with the 1st- and 2nd-order versions of the Roe and LD-HLL schemes on GR1 are shown in Fig. 2, together with the experimental data. As expected, both schemes introduce a larger dissipation at 1st order than in their 2nd-order version, as can be seen in particular from the lower predicted values of the suction peak. Note how at 1st order the LD-HLL scheme appears to be more dissipative than the Roe one, as also shown by the overestimation of C_p at the stagnation point. However at 2nd order the results obtained by the two different schemes are almost identical. As for accuracy, although there are no measurement points at the suction peak, a previously carried out potential flow simulation gave a suction peak value of approximately -1.7, in well agreement with simulations carried out with schemes of high-order of accuracy [21]. Thus, the predictions obtained with the 2nd-order versions of both considered schemes can definitely be considered as more accurate than those of the 1st-order ones. The small discrepancies observed near the trailing edge are due to the fact that the present simulations are inviscid and almost 2D; indeed, a similar behavior was observed in a 2D potential flow solution and in other Euler calculations in [21].

4.2.2 Results for cavitating conditions

A first important result of the cavitating test-cases is that the more complete time linearization is a key point to significantly increase numerical efficiency in presence of cavitation. Indeed, a CFL coefficient limitation of about 0.01 has been found for the Roe scheme and the LD-HLL one with the classical time linearization, while the more complete linearization permits to reach CFL 100 for the LD-HLL flux, both at first order and 2nd order of accuracy.

Therefore, only the simulations carried out with the most efficient approach, i.e. the LD-HLL one with the more complete time linearization, have been advanced in time sufficiently to obtain meaningful results. Note that an accurate prediction of the pressure near the leading edge and, in particular, of the suction peak is very important to correctly capture the cavitating region, which starts near the leading edge. The 1st-order version of the scheme, indeed, due to the underprediction of the suction peak, is not able to capture the cavitating region and gives no phase transition for the TC2 case. Consequently, also in accordance with the analysis carried in Sec. 4.2.1 for non-cavitating conditions, only 2nd-order accurate results are shown in the following (Figs. 3 and 4). Finally, two different grids are considered (GR2 and GR3), both more refined that the one used for the non-cavitating simulations. Fig. 3 shows the C_p distribution on the upper side of the hydrofoil obtained through numerical simulations (averaged values over 5000 time steps are shown) together with the relevant experimental data. The cavitation region is clearly visible and coincides with the C_p plateau near the leading edge. This behavior of pressure is typical of the adopted barotropic homogeneous-flow cavitation model, in which large density variations at almost constant pressure characterize the vapor regions (see, e.g., [1] or [3]). Note also the sharp pressure gradient at the vapor to liquid transition occurring at the end of the cavitation region, which also characterizes this type of cavitation models. Conversely, the wiggle observed at that location seems to be due to numerics and is indeed largely reduced by grid refinement, as can be seen from the comparison between the solutions obtained on GR2 and GR3 in Fig. 3a. This figure also shows that, except for this wiggle, grid independence of the results has been reached. To better highlight the behavior of the solution in the cavitation region predicted by the adopted barotropic homogeneous-flow model, Fig. 3b shows the evolution of the C_p curve with the cavitation number value obtained on the most refined grid, i.e. GR3. As expected, a decrease of the cavitation number corresponds to a larger cavitation region. Note also that in all cases the pressure is characterized by a plateau in this region, with a value increasing as the cavitation number decreases, and that a sharp gradient is always present at the vapor to liquid transition. The agreement with the experiments for the TC2 solution (the same inlet conditions as in the experiments) appears to be reasonable, although there are no experimental points in the plateau region and some discrepancy is present at the end of the cavitating region. However, based on the previous analysis, this discrepancy seems to be due more to modeling than to numerics.

Finally, in order to give an idea of the numerical stiffness, the iso-contours of the local cavitation number and of the Mach number obtained on grid GR3 for the TC3 case are shown in Fig. 4. The local cavitation number is defined as $\sigma = \dfrac{p - p_{sat}}{1/2\rho U_\infty^2}$; hence, negative values of σ identify the cavitation region (dark grey in Fig. 4). Note how in the cavitation region the Mach number reaches the value of 10, while the free-stream liquid flow value is equal to 2.4×10^{-3}, i.e. an increase of about 4 orders of magnitude.

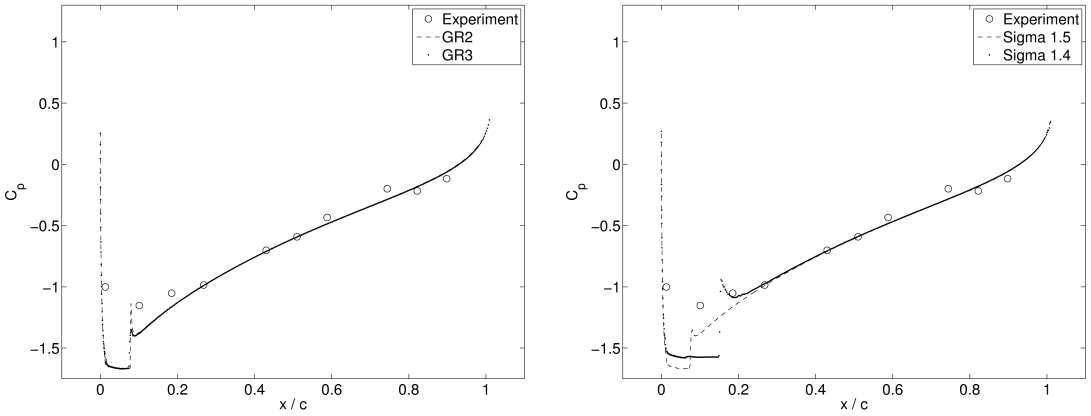

(a) (b)

Figure 3: C_p distribution for cavitating flow: a) different grid resolutions for TC2 test-case b) grid GR3: test-cases TC2 ($\sigma_\infty = 1.49$) and TC3 ($\sigma_\infty = 1.38$).

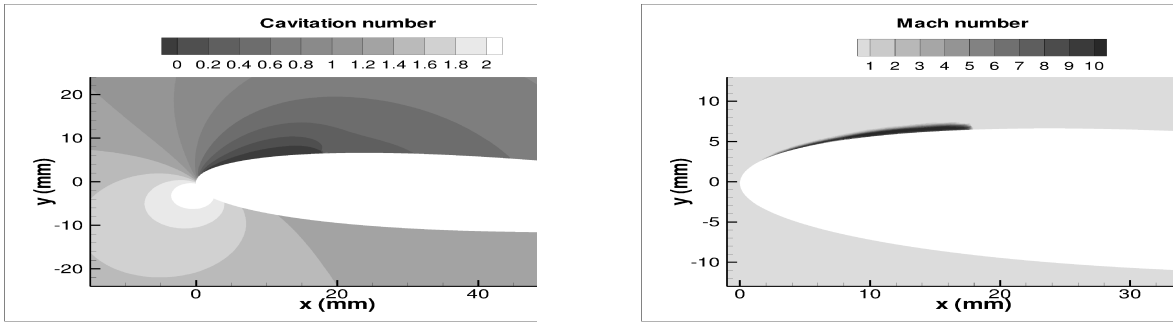

(a) (b)

Figure 4: Test-case TC3: time-averaged isocontours of (a) cavitation number and (b) Mach number.

5 CONCLUDING REMARKS

In the present study, a numerical formulation is proposed for the simulation of 3D viscous cavitating flows, which combines good properties of accuracy, robustness and efficiency. Since the chosen homogeneous-flow cavitation model leads to a complex barotropic state equation, the numerical schemes have been developed for generic barotropic flows. However, the simulation of cavitating flows, in particular for the chosen cavitation model, in which nearly-incompressible to supersonic regimes with huge variations of flow quantities have to be considered, leads to specific numerical difficulties from a view point of both accuracy and efficiency. The present approach is based on finite-volume and finite-element discretizations for convective and viscous terms respectively and relies on several ingredients introduced in previous works by the authors [6, 7, 13]. Compressible flows are considered and approximate Riemann solvers are used to compute finite-volume fluxes. Thus, suitable preconditioning is used to avoid accuracy problems in the low-Mach regime, while maintaining time consistency. Time advancing is carried out through a linearized implicit approach. However, in previous works it was found that the use of an implicit time advancing is not a sufficient guarantee when cavitation occurs; indeed, severe CFL limitations were observed for a linearized implicit formulation based on the Roe scheme [1]. Two new ingredients have been introduced here. First, a low-diffusive HLL numerical flux is proposed, which is obtained by introducing an anti-diffusive term in the Rusanov flux. Thanks to the particular features of the Riemann problem for cavitating flows, the simple structure of the Rusanov scheme could be maintained in the LD-HLL one. A suitable preconditioning for the low-Mach regime has also been defined. Second, two different time linearizations are considered for the LD-HLL flux; a classical one in which the upwind part of the flux function is partially frozen in the time differentiation, and a more complete one which takes into account, at least in an approximate way, the neglected term. Finally, second-order accuracy is obtained through a MUSCL reconstruction for space accuracy and a second-order backward differentiation formula for time advancing associated with defect-correction iterations.

The proposed numerical ingredients are validated through test-cases for which analytical solution or experimental results are available. Three different numerical flux functions adapted to barotropic flows, the Roe, Rusanov and LD-HLL ones, are compared, by including first- and second-order accurate formulations and the two kinds of linearization for the HLL-like schemes. The capability to obtain accurate solutions for viscous flows has been investigated considering as test-case the Blasius boundary layer over a flat plate. The results obtained for this test-case show that the anti-diffusive term introduced in the LD-HLL scheme is able to counteract the accuracy problem in presence of contact discontinuity. The suitability of this scheme for viscous flows is verified with a solution behavior very similar to the one of the Roe scheme and in good accordance with theoretical solution.

The simulation of a flow around a hydrofoil mounted in a tunnel has been consid-

ered in order to assess the accuracy, robustness and efficiency of the different numerical formulations in cavitating conditions. It clearly follows that the use of the more complete linearization is essential for efficiency in presence of cavitation. Indeed, very strong stability limitations appear when cavitation occurs, this for the Roe linearized implicit formulation as well as for the LD-HLL implicit approach using the classical linearization. An increase of four orders of magnitude is obtained in terms of CFL number, when the more complete linearization for the LD-HLL scheme is used. On another hand, good improvements have been observed by considering the second-order accurate approach with a behavior largely closer to experiments results and physical expectations. Thus, it emerges that the second-order preconditioned implicit LD-HLL approach associated to the more complete linearization appears an adequate formulation for viscous flows in cavitating conditions. It seems now, that the obtained numerical approach is enough efficient to be tested on real 3D industrial configurations of cavitating flows. Simulations of the flow in a realistic configuration of a rocket turbopump inducer in cavitating conditions are ongoing. Turbulence effects will also be included through RANS turbulence models.

Acknowledgments

The support of the European Space Agency under Contract no. 20081/06/NL/IA is gratefully acknowledged. The authors also wish to thank the Italian Computer Centers CINECA and CASPUR for having provided computational resources and support.

REFERENCES

[1] E. Sinibaldi. *Implicit preconditioned numerical schemes for the simulation of three-dimensional barotropic flows.* PhD thesis, Scuola Normale Superiore di Pisa, 2006.

[2] Y. Delannoy and J.L. Kueny. Cavity flow predictions based on the Euler equations. ASME Cavitation and Multiphase Flow Forum, pages 153–158, 1990.

[3] L. d'Agostino, E. Rapposelli, C. Pascarella, and A. Ciucci. A modified bubbly isenthalpic model for numerical simulation of cavitating flows. In 37^{th} *AIAA/ASME/SAE/ASEE Joint Propulsion Conference*, Salt Lake City, 2001.

[4] Q. Qin, C. Song, and R. Arndt. A virtual single-phase natural cavitation model and its application to CAV2003 hydrofoil. In *Proc. CAV2003*, Osaka, 2003.

[5] T. Liu, B. Khoo, and W. Xie. Isentropic one-fluid modelling of unsteady cavitating flow. *J. Comput. Phys.*, 201:80–108, 2004.

[6] E. Sinibaldi, F. Beux, and M.V. Salvetti. A numerical method for 3D barotropic flows in turbomachinery. *Flow Turbul. Combust.*, 76(4):371–381, 2006.

[7] E. Sinibaldi, F. Beux, M. Bilanceri, and M.V. Salvetti. *A Second-Order Linearised Implicit Formulation for Hyperbolic Conservation Laws, with Application to Barotropic Flows*. ADIA 2008-4. University of Pisa, June 2008.

[8] P. Roe. Approximate Riemann solvers, parameter vectors, and difference schemes. *J. Comput. Phys.*, 43:357–372, 1981.

[9] B. van Leer. Towards the ultimate conservative difference scheme V: a second-order sequel to Godunov's method. *J. Comput. Phys.*, 32(1):101–136, 1979.

[10] E. Goncalves and R. Fortes Patella. Numerical simulation of cavitating flows with homogeneous models. *Comp. Fluids*, 38:1682–1696, 2009.

[11] S. Davis. Simplified second-order Godunov-type methods. *SIAM J. Sci. Stat. Comput.*, 9(3):445–473, 1988.

[12] E. Toro. *Riemann solvers and numerical methods for fluid dynamics*. Springer, 1997.

[13] M. Bilanceri, F. Beux, and M.V. Salvetti. *Investigation on numerical schemes, preconditioning and time advancing in the simulation of 1D cavitating flows*. ADIA 2008-7. University of Pisa, October 2008.

[14] B. Einfeldt, C. Munz, P. Roe, and B. Sjögreen. On Godunov-type methods near low densities. *J. Comput. Phys.*, 92(2):273–295, 1991.

[15] S. Park and J. Kwon. On the dissipation mechanism of Godunov-type schemes. *J. Comput. Phys.*, 188(2):524–542, 2003.

[16] H. Yee. Construction of explicit and implicit symmetric TVD schemes and their applications. *J. Comput. Phys.*, 68(1):151–179, 1987.

[17] A. Cervone, C. Bramanti, E. Rapposelli, and L. d'Agostino. Thermal cavitation experiments on a NACA0015 hydrofoil. *J. Fluids Eng., Trans. ASME*, 128(2):326–331, 2006.

[18] A. Harten, P. Lax, and B. van Leer. On upstreaming differencing and Godunov-type schemes for hyperbolic conservation laws. *SIAM Rev.*, 25:35–61, 1983.

[19] H. Guillard and C. Viozat. On the behaviour of upwind schemes in the low Mach number limit. *Comp. Fluids*, 28:63–86, 1999.

[20] R. Martin and H. Guillard. A second-order defect correction scheme for unsteady problems. *Comp. Fluids*, 25(1):9–27, 1996.

[21] F. Beux, M.V. Salvetti, A. Ignatyev, D. Li, C. Merkle, and E. Sinibaldi. A numerical study of non-cavitating and cavitating liquid flow around a hydrofoil. *ESAIM:M2AN*, 39(3):577–590, 2005.